

COMMUNICATION

Dual reaction channels for photocatalytic oxidation of phenylmethanol on anatase†

Cite this: *Phys. Chem. Chem. Phys.*, 2013, **15**, 1082

Ye-Fei Li and Zhi-Pan Liu*

Received 6th September 2012,
Accepted 22nd November 2012

DOI: 10.1039/c2cp44137c

www.rsc.org/pccp

This work explores thoroughly the reaction network of the partial oxidation of phenylmethanol at the TiO₂-solvent interface under photocatalytic conditions by using a first-principles continuum solvation method. We demonstrate that the photocatalytic oxidation of phenylmethanol has a complex reaction network with dual pathways. The dimer pathway dominates the mechanism under aerobic conditions and a [C₆H₅CH(OH)O]₂ peroxy dimer is the key intermediate, the decomposition of which leads to an unusual O exchange phenomenon.

Recent years have seen intense interest in the selective conversion of organic chemicals *via* heterogeneous photocatalysis,^{1–3} which can be performed under mild and green reaction conditions. Photocatalysis has demonstrated unusually high selectivity for reactions such as the partial oxidation of alcohols and alkenes^{4–8} and the reduction of CO₂, which are otherwise challenging to achieve under traditional reaction conditions.^{9–13} However, due to combined complexity arising from the solid-liquid interface and the photoirradiation conditions, the knowledge framework on photocatalysis is still poorly established to date, and the understanding is often gleaned from thermally driven chemistry. New experimental and theoretical techniques are urgently called for to probe the reaction intermediates and understand the mechanism microscopically.

Although theoretical tools based on first principles calculations have demonstrated their great predictive power in thermally driven heterogeneous catalysis, the investigation of the kinetics of the photocatalytic process has long been frustrated because of the requirement for a simultaneous treatment under the photo-irradiation condition and on the solid-liquid interface.

Furthermore, the standard electronic structure methods for large solid systems, such as density functional theory (DFT) calculations, face difficulty in computing the band position of semiconducting materials. Without correct energy levels, the redox chemistry involving photo-generated holes and electrons cannot be correctly described.

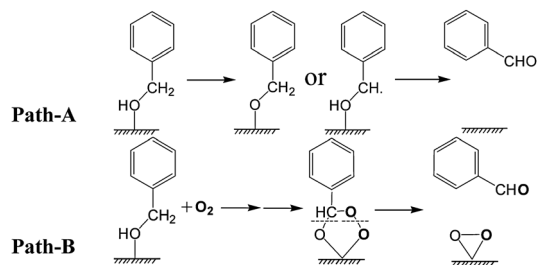
Aiming to probe the kinetics of photocatalysis in general, this work develops and applies new theoretical approaches to investigate an important photocatalytic system, namely, aerobic phenylmethanol oxidation on the anatase (101) surface in solution. Large-scale DFT calculation is combined with a periodic continuum solvation model based on the modified-Poisson-Boltzmann equation (CM-MPB) for modeling the charge-driven redox chemistry at the solid-liquid interface. A charged-slab approach based on DFT/CM-MPB, as outlined in the Appendix section, is designed and utilized to simulate the kinetics with excess holes and electrons on the surface. The calculation details and the methodology for calculating the photocatalytic kinetics are presented in the ESI† and our previous publication.¹⁴

To date, the mechanism of the photooxidation of the primary alcohols to aldehydes (RH₂COH + O₂ → RHCO + H₂O or H₂O₂) on TiO₂, although has been extensively studied in experiment,^{15–21} remains elusive. The high selectivity towards aldehydes is intriguing, implying that the reaction is kinetically controlled while the thermodynamically-favored deep oxidation products (*e.g.* acid, CO₂) can be avoided.²² It was often taken for granted that the phenylmethanol oxidation follows a step-wise dehydrogenation pathway (see Scheme 1, path-A) because there are some similarities between TiO₂ and metal catalysts.^{7,23–27} For example, TiO₂ is a poor catalyst for C–H or O–H bond activation under “dark” conditions (without photo-irradiation), similar to the gold catalyst. On the other hand, new evidence that has been emerging recently challenges the straightforward dehydrogenation mechanism. In particular, an unusual oxygen exchange phenomenon was observed by Zhang *et al.* using an isotope labeling technique.⁴ By analyzing the product of alcohols (*e.g.* C₆H₅CH₂OH, C₆H₁₁OH) photo-oxidation in organic solution,

Shanghai Key Laboratory of Molecular Catalysis and Innovative Materials,
Department of Chemistry, Key Laboratory of Computational Physical Science
(Ministry of Education), Fudan University, Shanghai 200433, China.

E-mail: zpliu@fudan.edu.cn; Fax: +86 21-6564-2400

† Electronic supplementary information (ESI) available: Calculation details and surface model; a theoretical approach for calculating the kinetics of photocatalytic reactions; structures and energetics of reaction pathways. See DOI: 10.1039/c2cp44137c



Scheme 1 The proposed pathways for phenylmethanol to benzaldehyde in the literature.^{4,28}

they found that the oxygen in the product (aldehydes/ketones) is from O_2 . They thus suggested a cyclic peroxo state as the intermediate (see Scheme 1, path-B) that is followed by a 1,3-O shift to produce aldehydes.

Here by exploring the likely reaction channels exhaustively, we identify dual reaction pathways for phenylmethanol partial oxidation, namely, the monomer and the dimer pathways, the preference of which depends critically on the availability of O_2 , as summarized in Scheme 2. The monomer pathway occurs only in the absence of O_2 , involving the sequential deprotonation of phenylmethanol, while the O_2 -assisted dimer pathway is responsible for the experimentally observed O isotope scrambling, featuring a superoxo $C_6H_5CH(OO)OH^*$ intermediate. Our new mechanism rationalizes the existing experimental findings and outlines the key factors for determining the photoactivity.

Our calculated free energy profiles of the pathways are shown in Fig. 1. In both pathways, the initial step is the same, namely $C_6H_5CH_2OH^* + h^+ \rightarrow C_6H_5CHOH^* + H^+(aq)$, in which the adsorbed phenylmethanol (state 1) is attacked by a photo-generated hole and experiences the α -CH bond breaking to

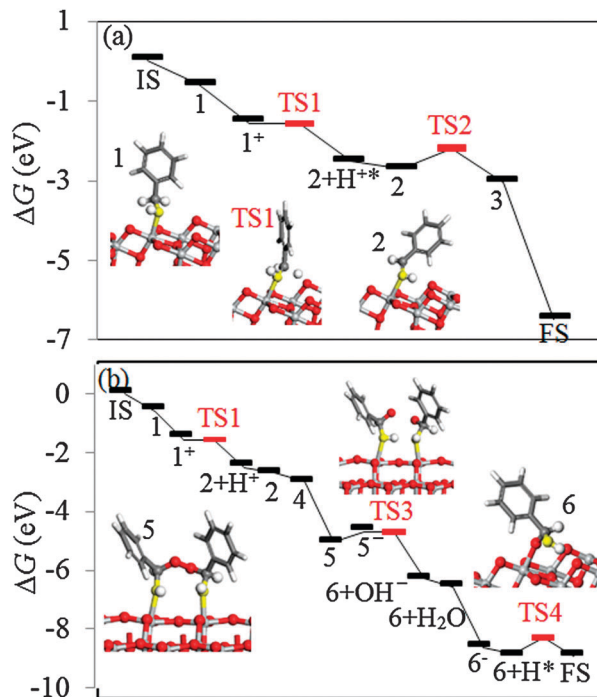
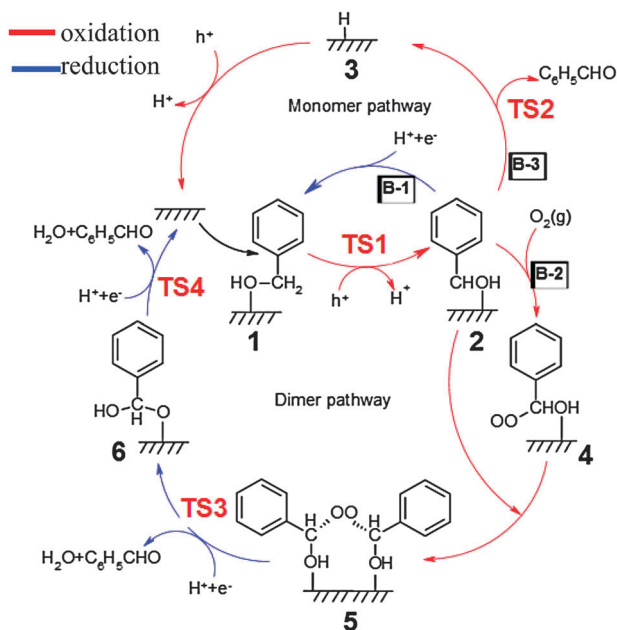


Fig. 1 The free energy profile for phenylmethanol oxidation via the monomer pathway (a) and the O_2 -assisted dimer pathways (b). The key intermediates are also illustrated (more shown in ESI†).

produce an adsorbed $C_6H_5CHOH^*$ radical (state 2). The positive charge originally on the hole is transferred to the dissociated proton after the reaction, which ends up with a solvated proton in aqueous solution. The free energy change of this step is calculated to be -2.15 eV. It is interestingly noticed that this value is considerably lower compared to that in H_2O splitting (the first OH bond breaking) on the same surface, -0.6 eV,¹⁴ indicating that H_2O splitting is substantially more difficult than the decomposition of the organic molecule.

It should be emphasized that the CH bond breaking reaction is kinetically driven by the surface hole. Without the surface hole, the reaction is highly activated with a barrier of 1.85 eV, unlikely to occur under ambient conditions. The hole driven bond breaking process can be decomposed into three elementary steps. (i) The hole transfer from the surface to the reactant, $C_6H_5CH_2OH^* + h^+ \rightarrow C_6H_5CH_2OH^{+*}$; (ii) the CH bond breaking by bypassing a transition state (TS1), $C_6H_5CH_2OH^{+*} \rightarrow C_6H_5CHOH^* + H^{+*}$; and finally (iii) the dissolution of the adsorbed proton, $H^{+*} \rightarrow H^+(aq)$. The free energies of the three steps from 1 to 2 are -0.96 , -0.96 and -0.23 eV (see Fig. 1). Remarkably, the reaction barrier for CH bond breaking is only 0.15 (in vacuum) and 0.19 eV (in water via CM-MPB), i.e. ~ 0 eV after ZPE correction, in the presence of a surface hole. The barrier of this step has also been examined using other density functionals: the calculated barrier under vacuum is 0.11 eV using the hybrid functional HSE06, which agrees with the value (0.15 eV) from the PBE functional.

In the monomer pathway, the C_6H_5CHOH radical continues to break its O–H bond to produce an adsorbed benzaldehyde



Scheme 2 The complete mechanism of phenylmethanol partial oxidation via the monomer pathway and the O_2 -assisted dimer pathway.

and H^* (state 3) by bypassing the **TS2** state, *i.e.* $C_6H_5CHOH^* \rightarrow C_6H_5CHO^* + H^*$. Our calculated barrier for the OH bond breaking is 0.52 eV (after ZPE correction). The bridging lattice O of the TiO_2 (101) surface helps to abstract the H from the C_6H_5CHOH radical, and after the reaction the H adsorbs on the lattice O yielding a reduced surface state. The benzaldehyde adsorbs only weakly on the surface ($E_{ad} = -0.23$ eV in aqueous surrounding) and can desorb from the surface. The remaining surface Hs will react with another hole to be released as a proton in solution (exothermic by 3.44 eV).

In the dimer pathway, the C_6H_5CHOH radical recombines with an O_2 molecule to form a superoxo radical,²² $C_6H_5CH(OO)OH^*$ (state 4) that is exothermic by 0.46 eV, *i.e.* $C_6H_5CHOH^* + O_2(g) \rightarrow C_6H_5CH(OO)OH^*$. The adsorbed superoxo molecule can then couple with another $C_6H_5CHOH^*$ radical to form a peroxo dimer $[C_6H_5CH(OH)O]_2^*$ (state 5) and the process is strongly exothermic by 1.88 eV. Such a radical coupling process is kinetically allowed by the low diffusion barrier (~ 0.2 eV) of the adsorbed $C_6H_5CH(OO)OH^*$ superoxo, which is apparently because it has two “legs” (the OO or the HO group) to bond with the surface Ti sites.

The subsequent steps in the dimer pathway are reduction steps driven by surface photoelectrons. Without the surface charge, the dimer complex $[C_6H_5CH(OH)O]_2^*$ is hard to decompose as the reaction barrier is more than 1 eV. By contrast, the reaction can occur *facilely via* $[C_6H_5CH(OH)O]_2^* + e^- \rightarrow [C_6H_5CH(OH)O]_2^{*-} \rightarrow C_6H_5CHO(aq) + OH^- + C_6H_5CH(OH)O^*$ and finally $OH^- + H^+(aq) \rightarrow H_2O(aq) + ^*$. The decomposition barrier (**TS3**) of the negatively-charged dimer $[C_6H_5CH(OH)O]_2^{*-}$ (state 5⁻) is very low, less than 0.1 eV. Next, $C_6H_5CH(OH)O^*$ (state 6) can readily decompose into benzaldehyde and water following a proton coupled electron transfer process, *i.e.* $C_6H_5CHOHO^* + e^- \rightarrow C_6H_5CHOHO^{*-}$ and $C_6H_5CHOHO^{*-} + H^+(aq) \rightarrow C_6H_5CHOHO^* + H^* \rightarrow C_6H_5CHO(aq) + H_2O(aq)$ (**TS4**). This reaction channel has an overall barrier of 0.57 eV, which is considerably lower than that of the direct decomposition of $C_6H_5CHOHO^{*-}$ to $C_6H_5CHO(aq)$ and OH^- , which has a barrier of 1.0 eV.

It should be mentioned that we also considered many other reaction channels, which are however less favorable compared to the two pathways above. For example, for the initial deprotonation, the OH bond breaking pathway was also considered. The calculated free energy change is -1.22 eV for $C_6H_5CH_2OH^* + h^+ \rightarrow C_6H_5CH_2O^* + H^+(aq)$, which is 0.93 eV higher than that of the CH bond breaking. Kinetically, it will also be shown later that the presence of the hole plays a key role in selectively breaking the CH bond.

The key kinetics steps in the reaction network of phenylmethanol oxidation can therefore be outlined, which is highlighted as **B-1**, **B-2** and **B-3** in Scheme 2, being the three possible branches starting from the radical product $C_6H_5CHOH^*$ and H^+ , after CH bond breaking. **B-1** is the reverse reaction back to phenylmethanol induced by a photoelectron. In the presence of a photo-electron, the radical product can be reduced that is endothermic by 0.23 eV, followed by a non-activated C–H bond formation to phenylmethanol. The net reaction is the

recombination of a hole and an electron (exothermic by 3.5 eV) mediated by the CH bond breaking/forming. **B-2** leads to the dimer pathway, where $C_6H_5CHOH^*$ recombines with $O_2(g)$ to generate the $C_6H_5CH(OO)OH^*$ radical. Due to the large entropy effect of O_2 in the gas phase, the adsorption of $O_2(g)$ needs to overcome a free energy barrier of 0.42 eV from DFT. **B-3** leads to the monomer pathway. $C_6H_5CHOH^*$ directly splits its OH bond to yield C_6H_5CHO and H^* , which has a reaction barrier of 0.52 eV.

Based on the energetics, we can tell that **B-1** (0.23 eV) is kinetically more favored than the other two branches (0.42 and 0.52 eV) that produce C_6H_5CHO . According to microkinetics, we can estimate that more than 99.9% product will recombine back to the reactant and only less than 0.1% $C_6H_5CHOH^*$ radical can be further oxidized under ambient conditions, assuming that photoelectrons are sufficiently available to access the product. It is therefore concluded that the low activity of the photocatalytic oxidation is not due to the presence of high barriers leading to the product, but mainly because of the facile reverse reaction at the first bond breaking step under the photo-irradiation conditions. To prevent the reverse reaction, the separation of the oxidation and the reduction sites in photocatalysis is therefore critical.

Our results show that the alcohol oxidation can switch from a monomer pathway to a dimer pathway by simply changing from the anaerobic to the aerobic conditions. This dual-pathway mechanism can reconcile some apparently contradictory findings in the field. Under the anaerobic conditions the oxidation of alcohols can proceed *via* electrochemistry (under the bias potential)⁴ or is assisted by metal cocatalysts (such as Pt and Ir co-catalysts on TiO_2).^{4,7} These conditions enable the removal of surface protons without the participation of O_2 . Under the aerobic conditions, the oxidation of alcohols proceeds with the dimer pathway, in which the O atom of benzaldehyde comes from the O_2 molecule instead of phenylmethanol, explaining the experimental finding by Zhang *et al.*⁴ The 1,3-O shift pathway (see Scheme 1, path-B) as suggested in the experimental study is however kinetically unlikely from our calculations since the calculated barrier is more than 1.5 eV, considerably higher than that of the dimer pathway identified in this work.

The above results have demonstrated that the first H removal in alcohol, *i.e.* CH bond breaking, is the key kinetics step that can only occur in the presence of a surface hole. It is intriguing why the hole selectively promotes the CH bond breaking, and not the OH bond breaking, considering that the initial OH bond breaking occurs more commonly on metal catalysts under heat driven conditions.²⁹ To answer this, we have examined how the barrier of the CH and OH cleavage varies upon the change of the surface charge by using the charged-slab method. The charge in the system is tuned gradually and at each fractional charge, n , the reaction barrier is calculated, as plotted in Fig. 2a. In general, both the CH and the OH cleavage reactions become facile with the increase in the surface positive charge. Interestingly, the slope of barriers against charge (*i.e.* $\partial E_a/\partial n$) for the C–H cleavage is much steeper

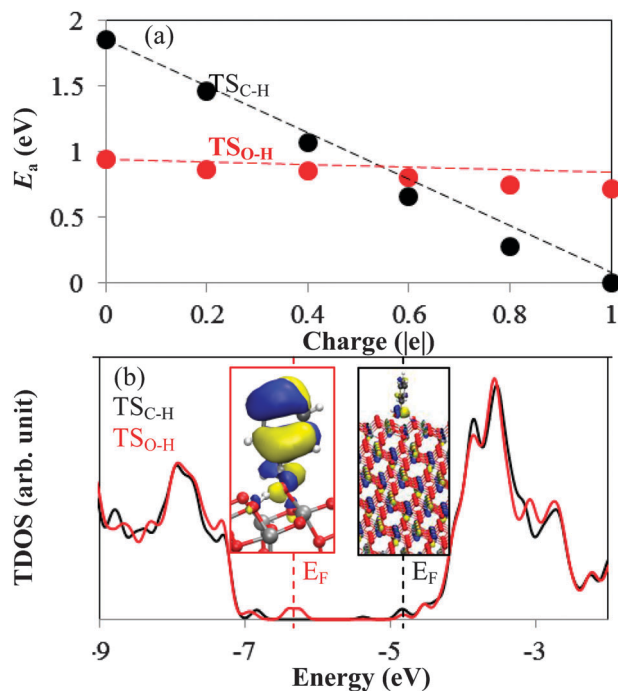


Fig. 2 (a) Calculated reaction barriers of the C–H (black) and the O–H (red) bond breaking of phenylmethanol under different surface charge conditions in aqueous surroundings. The dashed linear lines are plotted according to the calculated slope $\Delta\epsilon_{\text{HOMO}}$ under the charge-neutral condition (eqn (2)); (b) TDOSs of the TSs under the charge-neutral condition.

than that of the OH cleavage. While the CH bond breaking is much more difficult than the OH bond breaking in the absence of surface holes, at the +1 positive charge the CH bond breaking turns out to be the dominant reaction channel. The results show clearly that the presence of the surface hole can selectively promote the C–H bond breaking. But, why?

Quantitatively, the slope, $\partial E_a/\partial n$, can be written as a function of the eigenvalue of HOMO (ϵ_{HOMO}) at the IS and the TS based on the DFT theorem, which states that HOMO is the derivative of the free energy of electrons (G) to the number of electrons (N).^{30,31} It can be derived as eqn (1) and (2).

$$\begin{aligned} \frac{\Delta E_a}{\Delta n} &= \frac{E_a(N) - E_a(N - \Delta n)}{\Delta n} \\ &= \frac{E_{\text{TS}}(N) - E_{\text{TS}}(N - \Delta n)}{\Delta n} - \frac{E_{\text{IS}}(N) - E_{\text{IS}}(N - \Delta n)}{\Delta n} \end{aligned} \quad (1)$$

$$\frac{\partial E_a}{\partial n} \approx \epsilon_{\text{HOMO}}(\text{TS}) - \epsilon_{\text{HOMO}}(\text{IS}) = \Delta\epsilon_{\text{HOMO}} \quad (2)$$

where $\frac{E(N) - E(N - \Delta n)}{\Delta n} \approx \epsilon_{\text{HOMO}}$. Eqn (2) indicates that the larger the $\Delta\epsilon_{\text{HOMO}}$ under the charge-neutral condition (*i.e.* $n = 0$) is, the steeper the slope of the barrier would be. Indeed, using $\Delta\epsilon_{\text{HOMO}}$ as the slope in eqn (2) we can predict the correct trend for the change of the barrier against different surface charge conditions, as shown in Fig. 2a. Since the CH and OH bond breaking share the same IS, the difference in the slope must be attributed to the difference in the ϵ_{HOMO} (TS).

Indeed, by examining the electronic structure of the TS for the CH and OH bond breaking, we have found that the HOMO (E_F) of the CH bond breaking locates at the conduction band minimum (CBM), while the HOMO of the OH bond breaking locates in the gap, ~ 1 eV above the valence band maximum (VBM), as demonstrated in the calculated TDOS of the TS in Fig. 2b. The spatial distribution of the HOMO wave functions is shown in Fig. 2b. The different behavior in the HOMO distribution at the TSs can be understood as follows. For the CH bond breaking, it follows a homolytic bond breaking and the dissociated product is a C radical and H adsorbed on the surface under the neutral charge condition. The HOMOs are thus present on the H/TiO₂ (delocalized on the surface within the DFT-PBE framework) and on the C₆H₅CHOH radical, the energy of which is high and locates close to VBM (see Fig. 2b). On the other hand, the OH bond follows a heterolytic breaking and the dissociated product is a negatively charged C₆H₅CH₂O moiety and a surface adsorbed proton. The TS of OH bond breaking is thus more stable under the charge-neutral condition, the HOMOs of which locate mainly on the C₆H₅CH₂O moiety, being a gap state.

The above analyses make a clear distinction between the CH and OH bond activation on TiO₂ under photocatalytic conditions and the conclusion should be transferable to similar systems. Indeed, we also examined methanol decomposition on TiO₂ similarly. Our calculations show that without the surface charge, the CH bond breaking of methanol needs to overcome a barrier of 2.26 eV, while that for OH bond breaking is only 0.54 eV. In the presence of a surface hole, the CH bond breaking barrier drops significantly to zero, while the OH bond breaking still requires to overcome a small barrier (~ 0.1 eV). Although the CH bond breaking is not so strongly preferred in the case of methanol in the presence of a surface hole, the basic principle holds, *i.e.* the C–H bond breaking is selectively promoted under the photocatalytic conditions.

Conclusions

To recap, this work resolves the reaction network of a representative solid–liquid interface photocatalytic system at the atomic level, namely, the oxidation of phenylmethanol on anatase TiO₂ in solution. Unlike the thermally driven reaction, the aerobic photooxidation of the organic molecule is dominated by an unconventional dimeric pathway featuring radical coupling. The unique chemistry of photocatalysis is highlighted and rationalized, such as the selective CH bond activation and the charge recombination mediated by the chemical bond breakage/formation. Theoretical simulation also points out that the separation of the oxidation and the reduction sites is critical for improving photoactivity.

Appendix

The kinetic properties of photoreactions are sensitive to the position of VBM and CBM of the system, where the photo-generated hole and electron reside. However, because of the

well-known delocalization error in density functionals with local density approximation, the band gap of semiconductors directly borne from pure DFT calculations is generally underestimated, leading to the wrongly placed VBM and CBM.

Among the various methods proposed to correct the gap error, the recently-proposed Δ -sol method³² is an attractive approach, which utilizes the total energy of the charged periodic system to deduce the gap ($E_{\text{gap}} = E_{\text{CBM}} - E_{\text{VBM}}$), as written in eqn (3)–(5), without recourse to heavy-demanding high level quantum mechanics calculations. The Δ -sol method can reasonably avoid the delocalization error by confining the added charge to a volume that is commensurate with the range of the screening effects. The original method involves fitted parameters on the system size that were optimized for a set of bulk materials and thus cannot be easily applied for surface systems.

$$E_{\text{gap}} = [E(N_0 + n) + E(N_0 - n) - 2E(N_0)]/n \quad (3)$$

$$E_{\text{VBM}} = [E(N_0) - E(N_0 - n)]/n \quad (4)$$

$$E_{\text{CBM}} = [E(N_0 + n) - E(N_0)]/n \quad (5)$$

We here extend the idea to surface systems where the photocatalytic reactions occur. To do so, two key issues inherent to the charged-cell calculations must be properly addressed: (i) the image-charge interaction error due to the neutralizing counter-charge required in periodic system calculations; (ii) the optimum surface size (area) for the added charge on the surface. The image-charge interaction can in fact be largely avoided by using the DFT/CM-MPB approach because the neutralizing counter charge is distributed outside the surface region following the MPB equation and the large dielectric constant of water can effectively screen the image-charge interaction. To search for the optimum unit cell size for the surface system, we have calculated the band structure of a bare anatase $\text{TiO}_2(101)$ under different surface charge conditions from 0.13 to 1.13 e nm^{-2} (number of added charges divided by the surface area) and the corresponding $E_{\text{VBM}}/E_{\text{CBM}}$ are determined as plotted in Fig. 3. Fig. 3 shows that with the increase in the surface charge, the band gap increases, agreeing well with those found in bulk and finite systems.³² It is noticed that a window of the surface charge, *i.e.* 0.45–0.7 e nm^{-2} ,

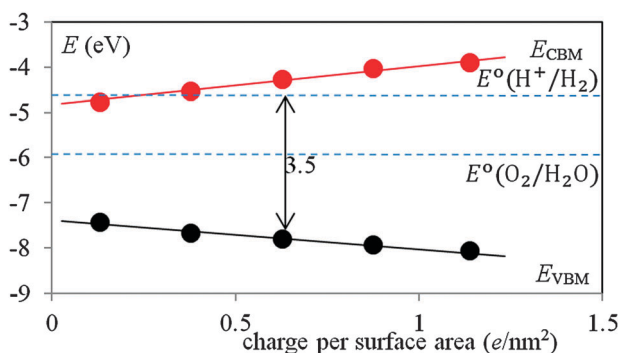


Fig. 3 The variation of the gap, E_{VBM} and E_{CBM} with respect to the added charge per surface area for anatase calculated using the charged-slab DFT/CM-MPB method.

can reproduce reasonably the experimental values ($E_{\text{gap}} \sim 3.2$ eV, $E_{\text{VBM}} \sim 3.0$ V vs. SHE and $E_{\text{CBM}} \sim -0.2$ V vs. SHE³³).

For photocatalytic reaction, the local surface charge however has to be one (either +1 or -1 from the hole/electron). In view of the 0.45–0.7 window, it is indicated that only certain size of the unit cell is allowed in order to reproduce the experimental values. In this work, we select a large rectangle unit cell (matrix notation $\begin{pmatrix} 4 & 0 \\ 1 & 2 \end{pmatrix}$, 10.398×15.264 Å), with which the predicted E_{gap} , E_{VBM} and E_{CBM} from charged-slab calculations with DFT-PBE functional are 3.5 eV, 3.2 V vs. SHE, -0.3 V vs. SHE, respectively. The surface charge is at 0.63 e nm^{-2} (Fig. 3) with the whole slab being explicitly charged by +2 or -2 (two exposed surfaces per slab). These values are generally close to the experimental data. The charged-slab approach allows the quantitative evaluation of the charge-driven reaction kinetics with reasonable VBM and CBM levels.

Acknowledgements

This work is supported by National Nature Science Foundation of China (20825311, 21173051), 973 program (2011CB808500, 2013CB834603), Science and Technology Commission of Shanghai Municipality (08DZ2270500). Dr. Jun Cheng and Dr. Liming Liu are acknowledged for the help on setting up CP2K calculations.

Notes and references

- C. Dai, J. M. R. Narayanan and C. R. J. Stephenson, *Nat. Chem.*, 2011, **3**, 140–145.
- T. P. Yoon, M. A. Ischay and J. Du, *Nat. Chem.*, 2010, **2**, 527–532.
- G. Palmisano, E. Garcia-Lopez, G. Marci, V. Loddo, S. Yurdakal, V. Augugliaro and L. Palmisano, *Chem. Commun.*, 2010, **46**, 7074–7089.
- M. Zhang, Q. Wang, C. Chen, L. Zang, W. Ma and J. Zhao, *Angew. Chem., Int. Ed.*, 2009, **48**, 6081–6084.
- Q. Wang, M. Zhang, C. Chen, W. Ma and J. Zhao, *Angew. Chem., Int. Ed.*, 2010, **49**, 7976–7979.
- W. Chen, F. N. Rein and R. C. Rocha, *Angew. Chem., Int. Ed.*, 2009, **48**, 9672–9675.
- W. Feng, G. Wu, L. Li and N. Guan, *Green Chem.*, 2011, **13**, 3265–3272.
- P. Kluson, H. Luskova, L. Cervený, J. Klisakova and T. Cajthaml, *J. Mol. Catal. A: Chem.*, 2005, **242**, 62–67.
- T. Inoue, A. Fujishima, S. Konishi and K. Honda, *Nature*, 1979, **277**, 637–638.
- W. C. Chueh, C. Falter, M. Abbott, D. Scipio, P. Furler, S. M. Haile and A. Steinfeld, *Science*, 2010, **330**, 1797–1801.
- K. Teramura, S. Iguchi, Y. Mizuno, T. Shishido and T. Tanaka, *Angew. Chem., Int. Ed.*, 2012, **51**, 8008–8011.
- S. S. Tan, L. Zou and E. Hu, *Catal. Today*, 2006, **115**, 269–273.
- Y. Shioya, K. Ikeue, M. Ogawa and M. Anpo, *Appl. Catal., A*, 2003, **254**, 251–259.
- Y.-F. Li, Z.-P. Liu, L. Liu and W. Gao, *J. Am. Chem. Soc.*, 2010, **132**, 13008–13015.
- V. Augugliaro, T. Caronna, V. Loddo, G. Marci, G. Palmisano, L. Palmisano and S. Yurdakal, *Chem.–Eur. J.*, 2008, **14**, 4640–4646.
- S. Higashimoto, N. Kitao, N. Yoshida, T. Sakura, M. Azuma, H. Ohue and Y. Sakata, *J. Catal.*, 2009, **266**, 279–285.
- S. Higashimoto, N. Suetsugu, M. Azuma, H. Ohue and Y. Sakata, *J. Catal.*, 2010, **274**, 76–83.
- G. Palmisano, S. Yurdakal, V. Augugliaro, V. Loddo and L. Palmisano, *Adv. Synth. Catal.*, 2007, **349**, 964–970.
- K. Ikeda, H. Sakai, R. Baba, K. Hashimoto and A. Fujishima, *J. Phys. Chem. B*, 1997, **101**, 2617–2620.

- 20 M. Fujihira, Y. Satoh and T. Osa, *Nature*, 1981, **293**, 206–208.
- 21 G.-M. Schwab, H. Noller, F. Steinbach and M. Venugopalan, *Nature*, 1962, **193**, 774–775.
- 22 A. Fujishima, T. N. Rao and D. A. Tryk, *J. Photochem. Photobiol., C*, 2000, **1**, 1–21.
- 23 K. Mori, T. Hara, T. Mizugaki, K. Ebitani and K. Kaneda, *J. Am. Chem. Soc.*, 2004, **126**, 10657–10666.
- 24 D. I. Enache, J. K. Edwards, P. Landon, B. Solsona-Espriu, A. F. Carley, A. A. Herzing, M. Watanabe, C. J. Kiely, D. W. Knight and G. J. Hutchings, *Science*, 2006, **311**, 362–365.
- 25 A. Villa, N. Janjic, P. Spontoni, D. Wang, D. S. Su and L. Prati, *Appl. Catal., A*, 2009, **364**, 221–228.
- 26 P. Haider, B. Kimmerle, F. Krumeich, W. Kleist, J.-D. Grunwaldt and A. Baiker, *Catal. Lett.*, 2008, **125**, 169–176.
- 27 J. Zhu, J. L. Figueiredo and J. L. Faria, *Catal. Commun.*, 2008, **9**, 2395–2397.
- 28 A. A. Ismail, L. Robben and D. W. Bahnemann, *ChemPhysChem*, 2011, **12**, 982–991.
- 29 C. Shang and Z.-P. Liu, *J. Am. Chem. Soc.*, 2011, **133**, 9938–9947.
- 30 W. Yang, Y. Zhang and P. W. Ayers, *Phys. Rev. Lett.*, 2000, **84**, 5172–5175.
- 31 J. P. Perdew, R. G. Parr, M. Levy and J. L. Balduz, Jr., *Phys. Rev. Lett.*, 1982, **49**, 1691–1694.
- 32 M. K. Y. Chan and G. Ceder, *Phys. Rev. Lett.*, 2010, **105**, 196403.
- 33 M. Gratzel, *Nature*, 2001, **414**, 338–344.